Enhanced Microgrid Performance using Coupled Inductor Switched Z-Source Boost Converter and GOA-Tuned RBFNN MPPT

A. A. Mohamed Faizal[1*] (iD), Nishant Dwivedi[2] (iD), M. Sivasubramanian[3] (iD), S. Marisargunam[4] (iD),

K. Rajesh[5] (iD), N. Janaki[6] (iD)

[1]Department of Electrical and Electronics Engineering, VV College of Engineering, Tisaiyanvilai, 628656, India

[2]Department of Electrical Engineering, Medi-Caps University, Indore, Madhya Pradesh.

[3]Department of Electrical and Electronics Engineering, Vel Tech Multi Tech Dr. Rangarajan Dr. Sakunthala Engineering College (Autonomous), Avadi, Chennai - 62.

[4]Department of Electrical and Electronics Engineering, Saveetha Engineering College (autonomous), Chennai - 602105, India.

[5]Department of Electrical and Electronics Engineering, NPR College of Engineering and Technology, Natham, Dindigul, Tamil Nadu, India.

[6]Department of Electrical and Electronics Engineering, Vels Institute of Science, Technology and Advanced Studies, Tamil Nadu, India.

(aamohamedfaizal106@gmail.com[1], nishant.dwivedi@medicaps.ac.in[2], shivam.annauniversity@gmail.com[3], sargunam.2010@gmail.com[4], rajeshk@nprcolleges.org[5], janaki.se@vistas.ac.in[6])

Corresponding Author; A. A. Mohamed Faizal, aamohamedfaizal106@gmail.com

Abstract- Microgrids are become increasingly prevalent in the near future because it serves a crucial purpose in incorporating Distributed Renewable Energy Resources (DRES) into the main grid. Because green power sources including Photovoltaic (PV) energy are weather sensitive, they are inclined to be exceedingly fluctuating. These resources, when combined with demand, might cause unsystematic disparities on both load and generation sides, necessitating the implementation of an efficient control strategy to ensure a consistent power supply to grid. Consequently, this research proposes a robust optimized Maximum Power Point Tracking (MPPT) based control approach with dc to dc converter for delivering the high stability with constant power supply to the microgrid. At the PV side, a Coupled Inductor Switched Z-Source Boost (CISZB) converter is deployed to assure constant current functioning via mode of microgrid linked inverter. The incorporation of Artificial Intelligence (AI) control methods for effective energy extraction improves the effectiveness of solar energy systems. As a result, a Grasshopper Optimisation Algorithm-based Radial Basis Function Neural Network (GOA-RBFNN) MPPT is presented to successfully extract the MPP in a PV array. Furthermore, this MPPT controller forecasts the duty factor of a CISZSB converter for the purpose of attaining the maximum power point. MATLAB/SIMULINK platform is utilized to simulate microgrid connected PV systems and functionality of the proposed system is determined with regard to MPP efficiency, and current Total Harmonic Distortion (THD).

Keywords- PV system microgrid, CISZB converter, GOA tuned RBFNN based MPPT, THD.

1. Introduction

The advancement of RES for power production has become necessary due to rising demands for electrical power, the fast depletion of petroleum and coal, and the dangers of rising temperatures and climate change [1, 2]. RES that provide renewable power with no greenhouse gases include hydropower, wind, solar, and geothermal [3, 4]. The Microgrid is a notion that has emerged as a consequence of expanding customer demand, dispersed generation, and more incorporation of sources of clean energy. Because it lowers emissions, network traffic, and losses of energy while increasing power reliability, effectiveness, and system stability, microgrids are advantageous for electricity consumers and grid administrators [5, 6]. Microgrids are categorized into three types: AC microgrids, DC microgrids, and hybrid AC/DC microgrids. [7-9].Amid these, DC microgrids are becoming more and more popular than typical AC microgrids because of a number of benefits, including the elimination of reactive power management, islanded mode

synchronisation and frequency incompatibilities [10]. The DC Microgrids are divided into grid-connected and islanded modes based on their operational characteristics.

PV power plant is one of the many types of RES that have experienced enormous expansion in the past few decades due to their accessibility and clean, emission-free energy output. The PV array output fluctuates over time and has small amplitude, therefore it is unable to transfer effectively to the grid-connected inverter [11-15]. Boost converters become necessary in order to control and increase the panel voltage [16, 17]. Consequently, as the effectiveness of the dc to dc converters greatly influences the system efficiency, appropriate converter has to be considered and implementation is essential. Due to fluctuating weather conditions, PV panels often have low generating voltages; therefore, converters are required to increase the voltage when connecting the solar array to a grid-linked inverter. Various converters, including the boost converter [18],Zeta converter [19], Cuk converter [20],SEPIC [21],buck boost converter [22], the switched Z source converter [23], bidirectional converter [24] and others, have been described as ways to enhance the DC-DC conversion process and achieve a regulated resultant voltage. While functioning at high duty cycles, converters like boost, Cukand buck-boost create substantial voltage gain along with elevated voltage stress across switches. MPPT operation of the CUK and SEPIC converters is hampered by the existence of significant input current ripples. However, a higher starting current, restricted voltage gain, increased voltage impact on components, discontinuous input, etc. are the main disadvantages of switched Z-source converter. This switched Z source network's shortcomings include high voltage stress, restricted boosting capability, and irregular current conduction. In an effort to address the issues listed above, this work develops the CISZSB converter, which offers high voltage gain with lower leakage reactance.

In PV system generation of electricity, the optimum power extraction technique is a primary factor to improve inconsistent solar irradiation and shading efficacy. Overall, a large number of control strategies have been put out for grid-coordinated photovoltaic systems [25, 26]. The widely utilised methods for MPPT in large and small PV applications are Perturb and Observe (P&O) and Incremental Conductance (InCond). Maintaining synchronisation, dependability, and overall system behaviour in a grid connection is a challenging problem [27, 28]. It has been proposed in [29] to use Fuzzy based MPPT to manage grid incorporated PV systems under fluctuating irradiance and load. PV energy generation has a higher efficiency than other sources; however it has a drift issue in unexpected weather. Hybrid Fuzzy approaches [30, 31] are also used for the tracking of solar power, but lack adaptability to highly dynamic conditions, such as rapid fluctuations in solar irradiance and temperature, since fuzzy logic relies on predefined membership functions that may not always generalize well. By evaluating varying step size for solar PV systems that are partially shadowed, ANN-based MPPT approach has been presented in [32]. Despite having a quick MPP approximation based on ANN capability and the PV array's specifications, its efficiency is quite low. Consequently, in order to alleviate the aforementioned difficulties in a PV system, an effective control mechanism is needed. Thus, to extract greater power from the PV system, a reliable GOA-tuned RBFNN-MPPT has been developed in this research work.

On the whole, conventional DC-DC converters suffer from limited voltage gain, which adversely impact efficiency and component reliability. Although these converters offer an alternative, they introduce issues like restricted boosting capability limiting their practical application. Furthermore, existing MPPT techniques face drawbacks such as tracking inaccuracies under rapidly changing irradiance, drift issues and poor adaptability to dynamic conditions. While hybrid Fuzzy approaches and ANN based MPPT methods have been explored, they exhibit tuning difficulties, computational complexity and inconsistent performance in varying shading scenarios. Moreover, maintaining grid synchronization, reliability and stability remains a challenge in PV-integrated microgrids. To bridge these gaps, there is a need for an optimized control strategy that enhances MPPT efficiency, ensures stable grid coordination and overcomes the limitations of traditional DC-DC converters.

To address the identified research gaps, this work proposes a robust GOA tuned RBFNN based MPPT integrated with a CISZSB converter for enhanced performance in PV based microgrid applications. The CISZSB converter is designed to effectively boost the PV generated DC voltage to the required level at the Point of Common Coupling while overcoming issues of limited boosting capability found in conventional converters. The GOA tuned RBFNN MPPT controller ensures fast and accurate tracking of the MPP, even under rapidly fluctuating irradiance and partial shading conditions compared to traditional MPPT techniques. By optimizing the energy extraction process and improving voltage stability, the proposed system significantly enhances efficiency and minimizes THD in grid-connected PV applications.

The work is designed as follows: section II deals with the explanation of proposed system, and section III analyses the modelling of proposed work. Section IV presents findings and evaluation of proposed work, with Section V offering conclusion.

2. Proposed System Description

Fig. 1 presents a visual illustration of the proposed control framework, it consists of PV panel connected to a CISZSB converter via a GOA adjusted RBFNN-based MPPT controller. At the output, a VSI and a synchronised single phase grid are linked.
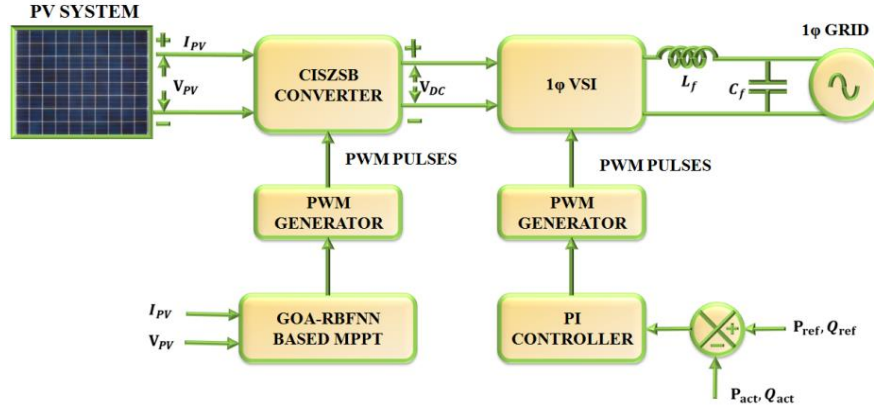
Fig. 1. PV based microgrid system using CISZSB converter with optimized MPPT.

The proposed system utilizes PV technology as a power generation source. To ensure that the output voltage meets operational requirements, a DC-DC converter is used to elevate PV voltage to a suitable level. A CISZSB converter is implemented for this purpose, offering both step-up and step-down functionalities. This converter demonstrates a wide range of output voltage, high reliability, and minimal inrush and fluctuation currents, making it an effective choice for application. To achieve MPPT, a GOA-assisted RBFNN is utilized. This strategy not only optimizes the power extraction from PV system but also enhances the performance of CISZSB converter. Converter's DC output is fed into a single-phase VSI, which converts DC voltage into AC voltage. PI controller is employed to ensure precise signal evaluation, using a reference input to minimize steady-state errors and prevent voltage fluctuations. Finally, inverter output is synchronized with grid, delivering high-quality power that meets grid standards. This system design ensures efficient power conversion, reliable performance, and integration with the electrical grid.

3. Proposed System Modelling

3.1. PV Modelling

PV systems are used extensively in generation of electricity. PV system is a semiconductor diode, which operates as the primary component and is exposed to solar radiation. When sunlight strikes the system, only a fraction of photons, each carrying varying levels of energy, interact with p-n junction. Photons with energy levels exceeding the material's band gap contribute energy equivalent to the band gap, while surplus energy is dissipated as heat. A schematic representation of the PV system is provided in Fig.2.
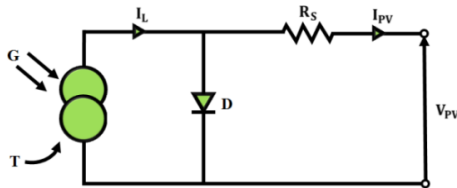

Fig. 2. PV equivalent circuit.

Where R_s and R_p stand for the PV system's series and parallel resistances, correspondingly. To simplify the process, R_p and R_s are removed because their values are too high and too low, respectively.

The following is a calculation of the PV solar system's V-I characteristic equation: PV system's photocurrent is provided by,

$$I_{pc} = [I_{si} + K_i(T - T_o)] * \frac{G}{1000} \qquad (1)$$

Where I_{pc}- Photo current, T is temperature in Kelvin, K_i is indicated by short circuit coefficient, T_o is reference temperature and G is solar irradiation.

PV arrays are typically joined in sets namely PV modules, and in a PV system, these are coupled in series or parallel to form PV arrays. The reverse saturation current of the module is provided by,

$$I_r = \frac{I_{si}}{\left[exp\left(\frac{qV_o}{N_s KnT}\right)-1\right]} \qquad (2)$$

Where, I_r- Reverse saturation current (A), I_{si}- Short circuit current (A), q is represents electron charge, V_o is indicated by output voltage, N_s is indicated by total count of PV cell connected in series, K- Boltzmann constant, n- Ideality factor of the diode and T- Operating temperature.

The PV module's current output is provided by,

$$I_{PV} = N_p * I_{pc} - N_p * I_s * \left[exp\left(\frac{\frac{V_{PV}}{N_s}+I_{PV}*\frac{R_s}{N_p}}{n*V_{th}}\right) - 1\right] - I_p \quad (3)$$

The CISZSB converter receives the output voltage from the PV system and further enhances the dc output voltage.

3.2. CISZSB Converter Modelling

The proposed converter employs a capacitor switch (C_2,D_2) in conjunction with capacitor division (C_1,D_1) in a conventional Z-source converter to generate a switched capacitor cell (C_1,C_2, D_1,D_2). With this configuration, the proposed converter obtains a higher voltage gain with less leakage reactance while conducting a continuous current.

To observe SZS converter's steady-state behaviour, the following two scenarios are proposed.

1. The parasitic impacts of switch, load resistance, diodes, capacitor and inductor are excluded on the assumption that the conditions are optimal.

2. In the Z-source converter, let $L1 = L2 = L$ and $C1 = C3 = C$, whereas in switched-capacitor cell, let $C1 = C2 = C3$, making $C1 = C2 = C3 = C$.

Two stages of operation are conceivable when proposed converter is operating in Continuous Current Mode (CCM), as presented in Fig. 3 (a) and (b).
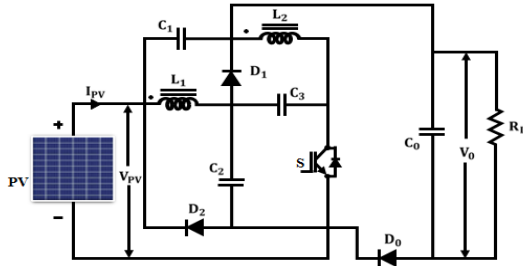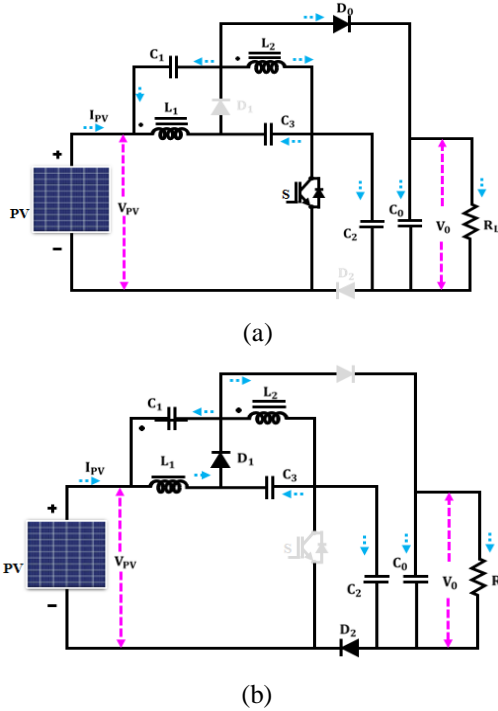

Fig. 3. Proposed CISZSB converter.

(a)

(b)

Fig. 4. (a) Stage I (b) Stage II.

a) Stage I:

Diodes D_1 and D_2 are opened when S is closed because they are connected antiparallel to capacitor. V_i and C_3 charge an inductance L_1, and L_2 is charged by V_i and C_1. V_i, C_1 and C_2 are linked in series, so switch S supplies power to load. Applying KVL, the following formulas are derived:

$$V_{L1} = V_{C3} + V_i, V_{L2} = V_{C1} + V_i \ and \ V_0 = V_{C1}, V_{C2} + V_i \quad (4)$$

Capacitances C_1 and C_3 are energised through L_1, L_2 and C_2 is energised since L_1 and V_i are series with L_2. The current passes via load through capacitor Co when S is released, D_1 and D_2 remain closed, and D_o is in an inverted blocking condition. The steady-state calculations that follow are $Vi = VL1 - VC3 + VC2, VL2 + VC3 = 0$, and $VL1 + VC1 =$

0. The normal voltage throughout the inductance in the constant state is "0," per the volt-time balancing criteria of the inductance. $D = Ton/Ts$, where Ton is the switch S's conduction duration and Ts is total switching time, is the formula for the duty percentage of a switch. Consequently,

$$V_{C1} = V_{C3} = \frac{D}{1-2D}V_i \quad (5)$$

$$V_{C2} = V_i + V_{C1} + V_{C3} = \frac{2-D}{1-2D}V_i \quad (6)$$

The output voltage V_0 is able to be obtained as a function of (5) and (6),

$$V_0 = V_i + V_{C1} + V_{C3} = \frac{2-D}{1-2D}V_i \quad (7)$$

Voltage gain (G) of CISZSB converter is calculated as follows:

$$G = \frac{V_0}{V_i} = \frac{2-D}{1-2D} \quad (8)$$

b) Stage II:

Similarly, when S is switched off in mode II, D_1 and D_2 open, allowing V_i and C_3 to charge L_1, V_i and C_1 to charge L_2. To supply current for the load in the interim, C_1 and C_2 are connected in series with V_i and C_3. By using KVL, the formulas that follow are able to derive. The formulas are as follows: $VL1 = Vi + VC3, VL2 = Vi + VC1$, and $V0 = Vi + VC1 + VC2 + VC3$. L_1 charges C_1 and C_2 in identical, L_2 charges C_3 and capacitor Co powers load when S is shut off. D_1 and D_2 are also activated. Diode Do is blocking the inductor as well. For this reason, $VL1 + VC1 = 0, VL1 + VC2 = 0$, and $VL2 + VC3 = 0$.

The subsequent formulas are derived employing the volt time equilibrium state of inductances L_1 and L_2:

$$V_{C1} = V_{C2} = V_{C3} = \frac{D}{1-2D}V_i \quad (9)$$

$$V_0 = V_i + V_{C1} + V_{C2} + V_{C3} = \frac{1+D}{1-2D}V_i \quad (10)$$

The resultant voltage gain is,

$$G = \frac{V_0}{V_i} = \frac{1+D}{1-2D} \quad (11)$$

In comparison to traditional DC-DC converters, the proposed CISZSB converter delivers superior outcomes and has many other benefits, such as a wider range of DC output voltage, excellent dependability and lower ripple currents.

3.3. GOA-RBFNN Based MPPT

The GOA tuned RBFNN-MPPT is adopted in this research to optimize power output from the PV panel. In addition, it is also used to enhance the efficiency of proposed CISZSB converter. The proposed MPPT controller is explained in depth in the section that follows.

3.4. RBFNN Based MPPT Controller

A cutting-edge and effective way to monitor a PV array's MPP is through the use of RBFNN method. With a benefit across the frequently employed multi-layer perceptron (MLP) network approach, which is created as a unification

determining nonlinear function of the scalar product of the input and weight vectors, RBFNN is possibly identified as a fitting curves task carried out in a multiple dimensions search domain. As a result, finding the surface that provides the greatest match to the training data in a multi-dimensional search space provides training challenge for constructed model.

As seen in Fig. 5, RBFNN is a three-layer network consisting of input, hidden, and output layers. The multidimensional vector M of PV array current (I_{ypv}), irradiance (Ir_y), and temperature (T_y) makes up the input layer in the present study. The duty cycle (D_y) is sole variable that has output layer N. The middle hidden layer conducts nonlinear change of input and has x radial basis functions (RBF) φ_k ($k = 1, 2, \ldots, x$).
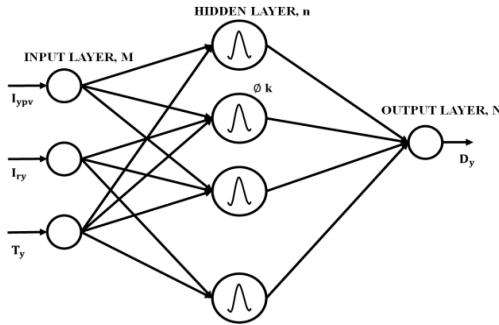

Fig. 5. RBFNN based MPPT.

The activation function is Gaussian function and the resultant layer establishes an additional space by mapping nonlinear properties using a linear combiner. For a dataset with n input variables, there are n hidden layers, one for every duty cycle value. Thus, (12) and (13) accomplish the input, output, and hidden layers.

$$M^y = \begin{bmatrix} Ir_y \\ T_y \\ I_{ypv} \end{bmatrix} \text{ and } N^y = D_y \ (y = 1,2,3 \ldots, n) \quad (12)$$

$$\varphi = \begin{pmatrix} \varphi_1^1 & \varphi_2^1 & \varphi_x^1 \\ \varphi_1^2 & \varphi_2^2 & \varphi_x^2 \\ \varphi_1^n & \varphi_2^n & \varphi_x^n \end{pmatrix} \quad (13)$$

At some point the nonlinear distribution is carried out by the function $\varphi_k(M^y)$. The frequently utilised Gaussian function, denoted by (14), is the formula used, where C_k indicates the φ_k centre with the identical dimension as is M^y and r is a scalar parameter that indicates the width of the RBF.

$$\varphi_k(M^y) = exp\left(\frac{\|M^y - C_k\|}{r^2}\right)^2 \quad (14)$$

As stated by (10), the output layer (N_l^y) in the PV array implementation is a continuously weighted total of the biases (b_k) and weighting factors (w_{kl}) of RBFs.

$$N_l^y = \sum_{k=1}^n w_{kl} \varphi_k(M^y) + b_k \quad (15)$$

This Gaussian function strategy gets around large computing demands and statistical difficulty by ensuring that the distribution of input parameters is linear to hidden layer. With a spread factor of 1, an orthogonal least squares

technique is used to train RBFNN controller. For function fitting, Gaussian neurons are controlled by spread factor value. The function becomes better if spread constant is large; however, an excessive value might demand more neurons to fit the rapidly changing function, whilst a tiny spread may cause overfitting. Thus, it ought to be handled with cautiousness.

3.5. Grasshopper Optimization Algorithm

The GOA models the way insects in the wild forage for food in an effort to identify the best solutions to challenging mathematical and even practical challenges.

$$X_i = S_i + G_i + A_i \quad (16)$$

The insects path of flight naturally served as the model for this technique: X_i represents the grasshopper's position, S_i represents social interaction, G_i denotes gravitational pull acting on it, and A_i denotes horizontal force acting on the grasshopper's direction of motion. Given that the GOA's primary search method is social interaction, which is examined by:

$$S_i = \sum_{j=1, j\neq i}^N s(d_{ij}) \hat{d}_{ij} \quad (17)$$

The amount of space between the ith and jth grasshopper, d_{ij} is determined in reference to (16) by using the formula $dij = |xj - xi|$. Furthermore, $\hat{d}_{ij}$ is a unique vector that connects the ith grasshopper to the jth grasshopper and It is possible to computed as follows: $\hat{d}ij = \frac{xj - xi}{dij}$.

The path of the locust in the congested is stated as follows, assuming the apparent position of the primary component S in Eq. (16):

$$s(r) = fe^{\frac{-r}{l}} - e^{-r} \quad (18)$$

Eqs. (19) and (20) yield the elements G and A that stand for the locust's gravity force and the wind's horizontal force, as follows:

$$G_i = -g\hat{e}_g \quad (19)$$

In Eq. (19), g represents the gravitational constant, while $\hat{eg}$ denotes a single vector pointing towards the Earth's centre.

$$A_i = u\hat{e}_w \quad (20)$$

Where $e\hat{w}$ is a single vector in the path of the breeze and u is the drifted variable.

Mathematically, the locust optimisation algorithm appears as follows:

$$X_i^d = c\left(\sum_{j=1, j\neq i}^N c\frac{ub_d - lb_d}{s} s\left(\left|x_j^d - x_i^d\right|\right)\frac{x_j - x_i}{d_{ij}}\right) + \hat{T}_d \quad (21)$$

Where optimal solution is represented by $\hat{T}_d$, c is the subtracting factor to lessen the ease of use, attraction, and gravitational areas, and ub_d and lb_d are the upper and lower limits of d, correspondingly.

In Eq. (21), $s(|xjd - xid|)$ specifies whether a grasshopper ought to be incorporated into or rejected from the target. $\frac{ub_d - lb_d}{s}$ is an equation that progressively minimises the

space that grasshoppers require for exploration and exploitation. The GOA's controller, variable c, is calculated as follows:

$$c = cmax - l\frac{cmax - cmin}{L} \tag{22}$$

The minimum and maximum values of c are denoted by symbols $cmax$ and $cmin$, respectively, in Eq. (22).

3.6. Single Phase VSI (Voltage Source Inverter)

The output of the CISZSB converter is received by the single phase VSI, which then transform a fixed voltage from a system like a DC power supply to an evolving frequency AC supply. Fig.6 shows circuit schematic for VSI that is connected to the grid.
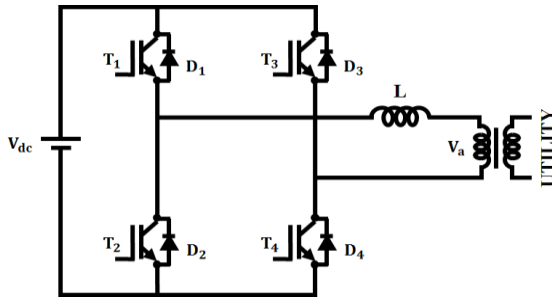

Fig. 6. Single phase VSI.

The PWM generator produces pulses needed for VSI, and inverter is made up of switches $T_1, T_2, T_3,$ and $T_4,$. Grid synchronisation involves analogization of reference and actual powers using a PI controller. The inverter provides grid with higher-quality power at acceptable variances in voltage, frequency, and phase angle because of synchronisation. Consequently, output in the single phase grid is of a superior integrated voltage.

4. Results and Discussion

An efficient GOA adapted RBFNN-based MPPT with CISZSB converter for improving the reliability of PV-based microgrid applications is proposed in this work. The CISZSB converter's aim is to boost the PV DC voltage to the identical level of DC voltage at the PCC. The proposed MPPT controller approach efficiently tracks maximum power from PV panel. The system has been verified with MATLAB software, and excellent outcomes are obtained, the Table 1 represents parameter specifications of proposed work.

Table 1. Description of parameters

Parameter	Specification
PV System	
Short Circuit Current	8.33A
Series connected solar PV c	36
Peak Power	10KW, 10 Panels
Open Circuit Voltage	12V
Coupled Inductor Interleaved SEPIC Converter	
Winding 1 Self Impedance	
$L_1(H)$	1.1 mH
$R_1(ohm)$	1.1
Winding 2 Self Impedance	
$L_2(H)$	1.1 mH
$R_2(ohm)$	1.1
C_1, C_2, C_3	22μF
C_o	2200μF

Case 1: At Variation of Temperature and Intensity

The computed waveforms for PV factors such temperature, voltage, irradiance and current are shown in Fig. 7. The temperature goes up from 25°C to 35°C in 0.3s, whereas the radiation from PV increases from 800W/m2 to 1000W/m2 in the same duration of time. An output that is controlled to 58 V and 70 A is determined after 0.3 seconds.
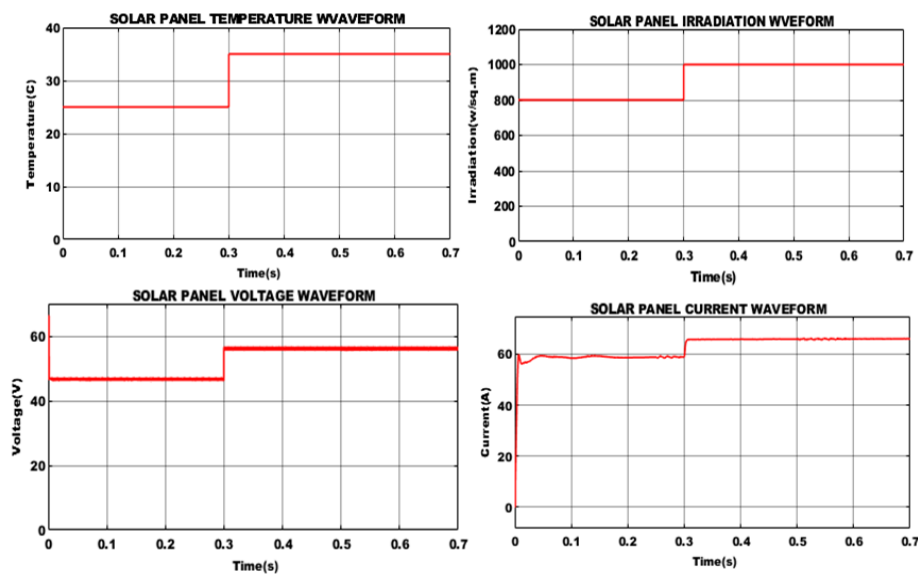

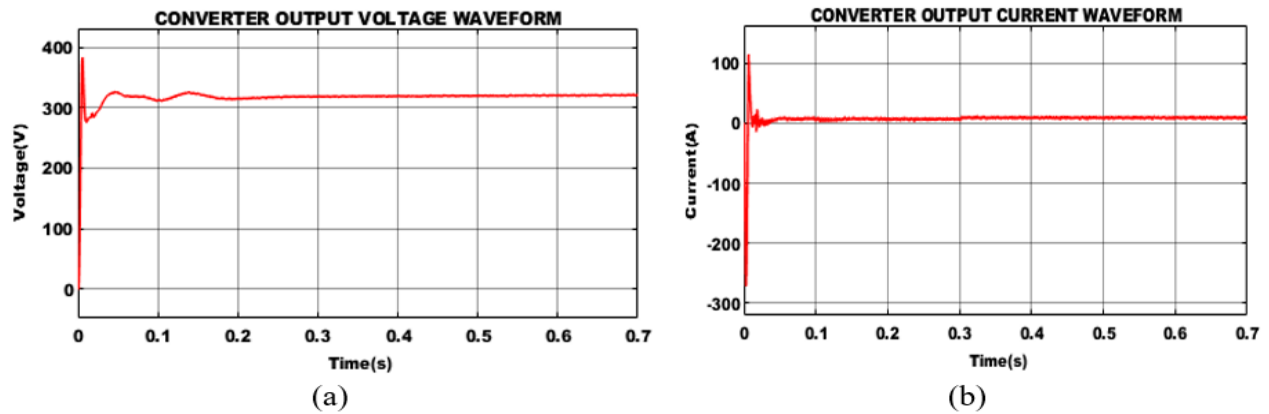**Fig. 7.** PV panel parameters at variation case.

Fig. 8. CISZSB converter output.

The proposed coupled inductor switched Z source boost converter resultant current and voltage waveforms are depicted in Fig.7. From observation is it clear that, the stable voltage of 320V is obtained with minor distortions, likewise, current remains constant at 20 Amps after 0.3 seconds. A PI controller, which generates a controlled output to assist eliminate distortions, regulates the output of the inverter.Fig.8 displays the output waveforms of the grid parameters, which include voltage, current, real, and reactive parameters. The waveform unambiguously demonstrates that while reactive power is zero, the real power first increases and dips before stabilising at a constant value. Similarly, the constant voltage 230V and 20 Amps currents are maintained respectively as seen Fig.9.
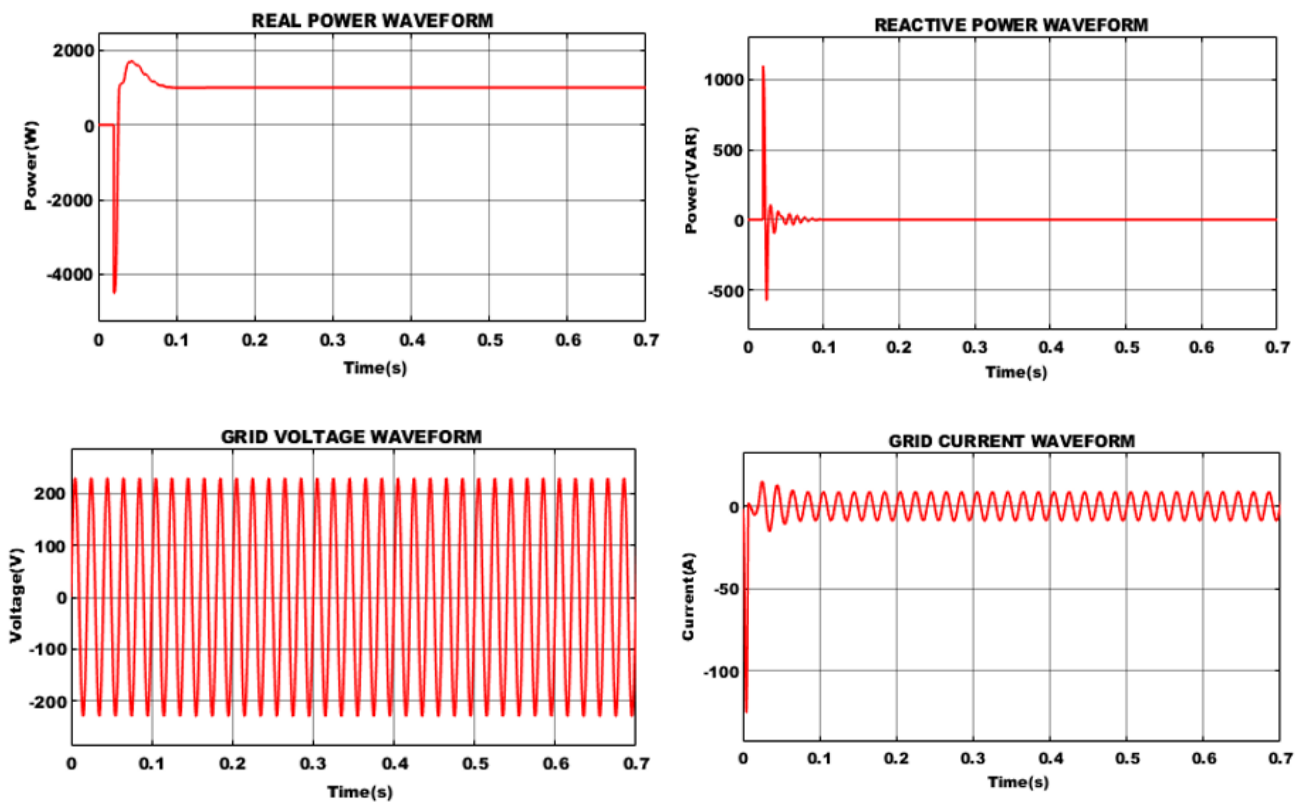

Fig. 9. Output waveforms of grid parameters.

Case 2: At Constant Temperature and Intensity

PV system's voltage, current, temperature, and irradiance are shown in Fig.10. A constant temperature of 35°C and an irradiation value of 1000 W/Sqare noticed. Similarly, a steady voltage of 58V is reached, and it took 0.3 seconds for the current to maintain a 70 Amps level.
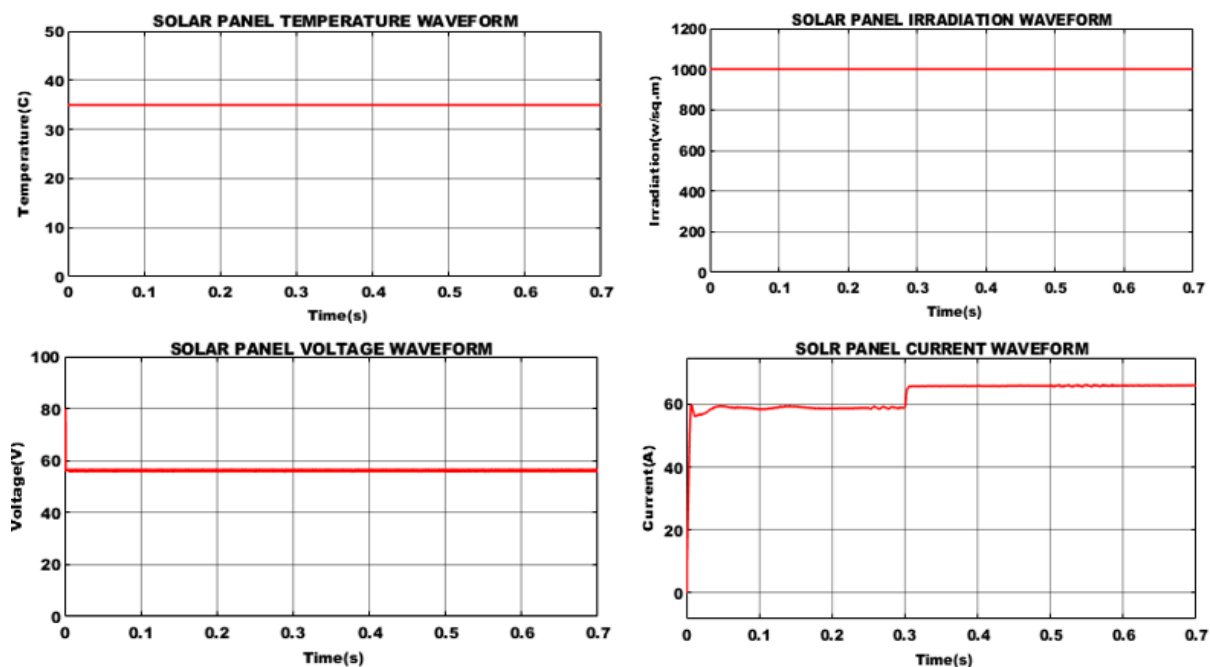
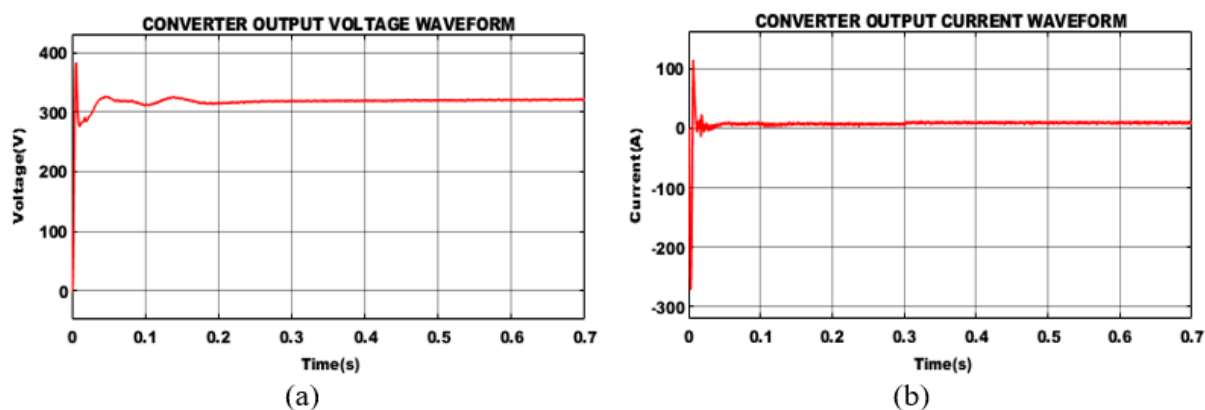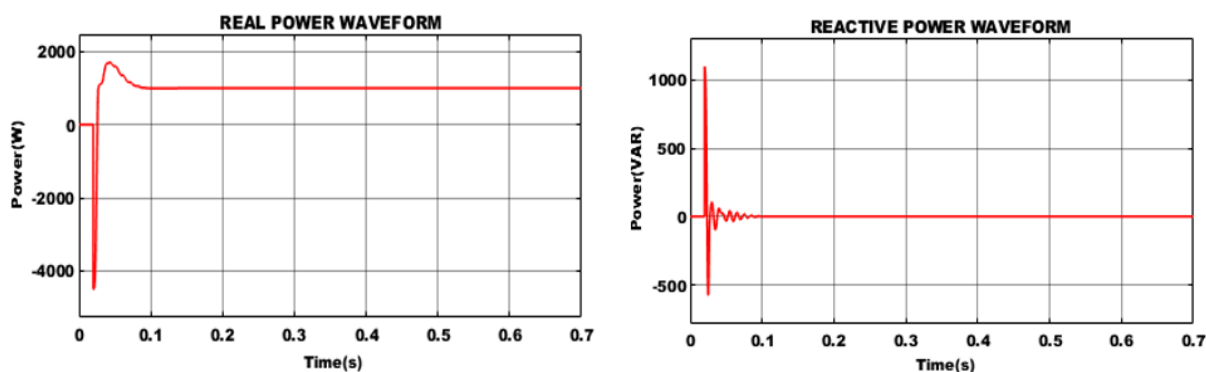**Fig. 10.** PV panel parameters at constant case.

Fig. 11. Output voltage and current waveforms of CISZSB converter.

Fig.11 represents the proposed CISZSB output under case 2 condition. It is evident that a steady voltage of 320V is achieved with minimal aberrations, and after 0.3 seconds, the current is fixed at 20 Amps.
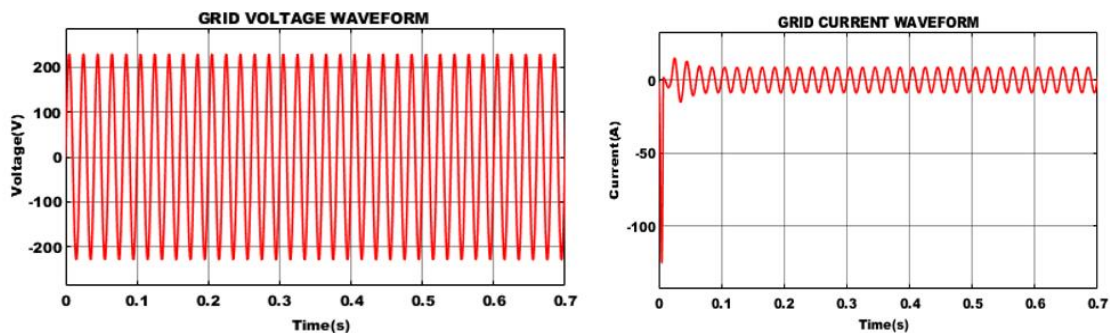
Fig. 12. Output waveforms of grid parameters.

Fig. 12 displays the resulting waveforms of the grid variables, comprising voltage, current, real, and reactive parameters. The waveform clearly shows that actual power first rises and falls before settling at an unchanged value, whereas reactive power is zero. As observed in Fig.12, constant voltage of 230V and current of 20 Amps were also maintained.
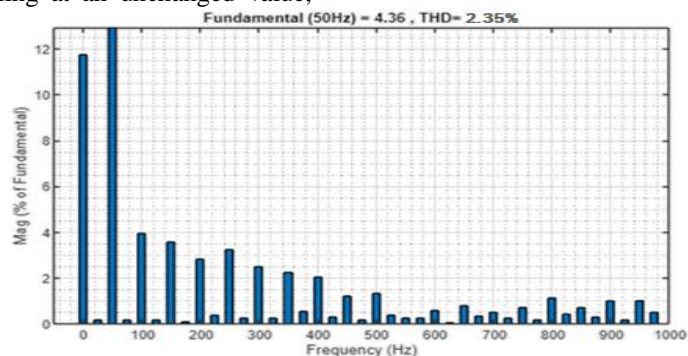

Fig. 13. THD waveform.

Total harmonic distortion (THD) has been significantly decreased in the proposed work; its value is stated as 2.35%, and Fig. 13 shows the depiction of THD.

Converters	Efficiency
Boost	80% [33]
Cuk	85 %[34]
SEPIC	88.82% [35]
Z − source converter	93.5 %[36]
Proposed converter	94.7
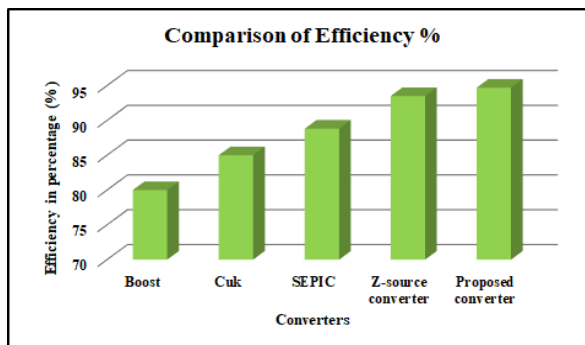
Fig. 14. Comparison of efficiency.

MPPT	Tracking Efficiency
P&O [37]	90.5%
INC [38]	96%
Fuzzy [39]	97.79%
GOA-RBFNN based MPPT	98.1 %
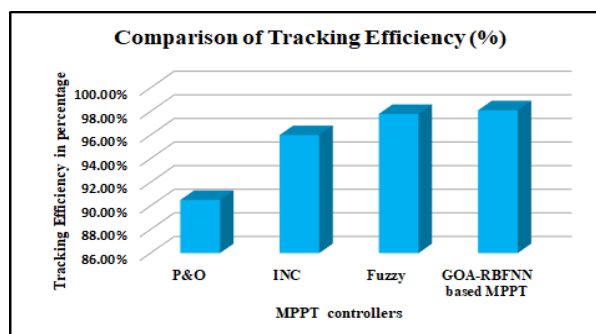
Fig. 15. Comparison of tracking efficiency.

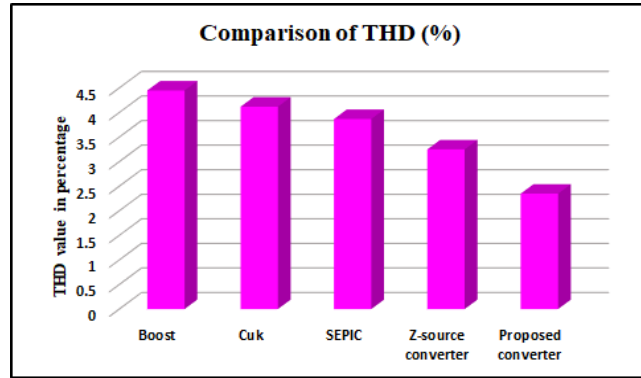| Converters	THD (%)
Boost	4.45
Cuk	4.12
SEPIC	3.87
Z-source converter	3.25
Proposed converter	2.35

Fig. 16. Comparison of THD.

The graphical representations of MPPT controller and converter efficiency are presented in Fig. 14 and 15. Considering an improved efficiency value of 94.7%, the proposed CISZSB converter functions significantly better than the traditional converters listed in [33], [34], [35] and [36]. The GOA-RBFNN controller has 98.1% efficiency, which is comparable to how MPPT efficiency has been increased. Compared to the controllers' efficiency numbers stated in [37], [38] and [39], this efficiency is noticeably higher. The THD graphic representation of the proposed work is presented in Fig.16, demonstrating that system has a minimised THD value of 2.35%.

Table 2. Comparison of computational complexity

MPPT algorithm	Computational complexity	Significance
PSO-ANN	$O(N \times d \times L \times I)$	Higher complexity
PSO-RBFNN	$O(N \times d \times M)$	Moderate complexity, slower convergence
GOA-ANN	$O(N \times d \times L \times I)$	Higher complexity, better performance
GOA-RBFNN	$O(N \times d \times M)$	Balanced computational cost and faster convergence

Table 2 represents the comparison of computational complexity of the GOA-RBFNN with other related MPPT algorithms like Particle Swarm Optimization (PSO). Here, N-number of particles/grasshoppers, d-dimensionality of search space, L-number of ANN layers, I-number of iterations, M-number of RBF neurons. The comparative analysis indicates that GOA-RBFNN exhibits balanced characteristics between computational cost and convergence. GOA dynamically modifies its search behavior, in contrast to conventional metaheuristic algorithms, enabling quick initial convergence through extensive exploration while progressively improving solutions for increased accuracy. This flexibility guarantees that GOA identifies the ideal power point quickly while remaining resilient against local optima, even under changing circumstances. By using the social interaction coefficient to balance exploration and exploitation, GOA improves stability and efficiency over the long run.

5. Conclusion

This paper proposes a reliable, optimised MPPT-based control strategy with a converter to provide microgrid with a high level of stability and a steady power supply. Utilising a grid-linked inverter mode, a CISZB converter is installed at the PV side to ensure stable current functioning. Solar energy systems are more effective when AI control techniques are used for efficient energy extraction. Consequently, an MPPT that is based on GOA-RBFNN is demonstrated to effectively track the MPP in a PV array. In addition, this MPPT controller predicts a CISZSB converter's duty factor in order to achieve the MPP. The proposed system's performance and microgrid-connected PV installations are simulated using the MATLAB/SIMULINK platform. Finally, excellent results are produced for power management, which has a 92% increased efficiency, 98.1% tracking efficiency, and a 2.35% total harmonic distortion (THD) value, respectively. The proposed work can be extended in future with the inclusion of hybrid renewable energy sources enhancing its versatility.

References

[1] K. S. Kavin, P. S. Karuvelam, A. Pathak, T. R. Premila, R. Hemalatha, and T. Kumar, "Modelling and Analysis of Hybrid Fuzzy Tuned PI Controller based PMBLDC Motor for Electric Vehicle Applications," SSRG International Journal of Electrical and Electronics Engineering, vol. 10, no. 2, pp. 8–18, 2023.

[2] K. S. Kavin, and P. S. Karuvelam, "PV-based Grid Interactive PMBLDC Electric Vehicle with High Gain Interleaved DC-DC SEPIC Converter," IETE Journal of Research, vol. 67, no. 7, pp. 4791–4805, September 2023.

[3] A. M. Mahfuz-Ur-Rahman, Islam, M. R. Muttaqi, K. M. and Sutanto, D. "An effective energy management with advanced converter and control for a PV-battery storage based microgrid to improve energy resiliency," IEEE Transactions on Industry Applications, vol. 57, no. 6, pp. 6659–6668, September 2021.

[4] R. Bakhshi-Jafarabadi, J. Sadeh, J. de Jesus Chavez, and M. Popov, "Two-level islanding detection method for grid-connected photovoltaic system-based microgrid with small non-detection zone," IEEE Transactions on Smart Grid, vol. 12, no. 2, pp. 1063–1072, October 2020.

[5] Y. Yang, Y. Qin, S. C. Tan, and S. Y. R. Hui, "Efficient improvement of photovoltaic-battery systems in standalone DC microgrids using a local hierarchical control for the battery system," IEEE Transactions on Power Electronics, vol. 34, no. 11, pp. 10796–10807, February 2019.

[6] Z. Li, Z. Cheng, J. Si, S. Zhang, L. Dong, S. Li, and Y. Gao, "Adaptive power point tracking control of PV system for primary frequency regulation of AC microgrid with high PV integration," IEEE Transactions on Power Systems, vol. 36, no. 4, pp. 3129–3141, January 2021.

[7] H. W. Yan, A. Narang, H. D. Tafti, G. G. Farivar, S. Ceballos, and J. Pou, "Minimizing energy storage utilization in a stand-alone DC microgrid using photovoltaic flexible power control," IEEE Transactions on Smart Grid, vol. 12, no. 5, pp. 3755–3764, April 2021.

[8] F. R. Badal, S. K. Sarker, S. R. Fahim, S. K. Das, M. R. Islam, A. Z. Kouzani, and M. P. Mahmud, "Robust controller design for tracking enhancement of a grid-tied pv-battery microgrid under industrial loads," IEEE Transactions on Applied Superconductivity, vol. 31, no. 8, pp. 1–5, August 2021.

[9] H. R. Baghaee, D. Mlakić, S. Nikolovski, and T. Dragicčvić, "Anti-islanding protection of PV-based microgrids consisting of PHEVs using SVMs," IEEE Transactions on Smart Grid, vol. 11, no. 1, pp. 483–500, June 2019.

[10] S. Pannala, N. Patari, A. K. Srivastava, and N. P. Padhy, "Effective control and management scheme for isolated and grid connected DC microgrid," IEEE Transactions on Industry Applications, vol. 56, no. 6, pp. 6767–6780, 2020.

[11] A. Zabihi, I. Sadeghkhani and B. Fani, "A partial shading detection algorithm for photovoltaic generation systems," Journal of Solar Energy Research, vol. 6, no. 1, pp. 678-687, 2021.

[12] A. Zabihi, M. Parhamfar, S. S. Duvvuri and M. Abtahi, "Increase power output and radiation in photovoltaic systems by installing mirrors," Measurement: Sensors, vol. 31, pp. 100946, 2024.

[13] M. Parhamfar and A. Zabihi, "Comprehensive Design of a 100-Kilowatt Solar Power Plant with Bifacial Technology in PVsyst for Arak, Iran," Solar Energy Advances, pp. 100092, 2025.

[14] S. Nasef, A. Hassan, H. ElMadany, M. Zahran, M. EL-Shaer and A. Abdelaziz, "Optimal power management and control of hybrid photovoltaic-battery for grid-connected doubly-fed induction generator based wind energy conversion system," International Journal of Renewable Energy Research, vol. 12, no. 1, pp. 408-421, 2022.

[15] A. Cordeiro, M. Chaves, H. Canacsinh, R. Luís, V. F. Pires, D. Foito, A. J. Pires and J. F. Martins, "Hybrid Sepic-Cuk DC-DC converter associated to a SRM drive for a solar PV powered water pumping system," In 2019 8th International Conference on Renewable Energy Research and Applications (ICRERA), pp. 169-174. IEEE, 2019.

[16] M. S. Bhaskar, M. Meraj, A. Iqbal, S. Padmanaban, P. K. Maroti, and R. Alammari, "High gain transformer-less double-duty-triple-mode DC/DC converter for DC microgrid," IEEE Access, vol. 7, pp. 36353–36370, August 2019.

[17] A. A. Saafan, V. Khadkikar, M .S. El Moursi, and H. H. Zeineldin, "A new multiport DC-DC converter for DC microgrid applications," IEEE Transactions on Industry Applications, vol. 59, no. 1, pp. 601–611, October 2022.

[18] D. Bao, A. Kumar, X. Pan, X. Xiong, A. R. Beig, and S. K. Singh, "Switched Inductor Double Switch High Gain DC-DC Converter for Renewable Applications," IEEE Access, vol. 9, pp. 14259–14270, January 2021.

[19] A. A. Dionizio, L. P. Sampaio, S. A. O. da Silva, and S. D. J. M. Machado, "Grid-Tied Single-Phase Integrated Zeta Inverter for Photovoltaic Applications," Energies, vol. 16, no. 9, pp. 3622, April 2023.

[20] J. C. D. S. de Morais, J. L. D. S. de Morais, and R. Gules, "Photovoltaic AC Module based on a Cuk Converter with a Switched-Inductor Structure," IEEE Transactions on Industrial Electronics, vol. 66, pp. 3881–3890, July 2019.

[21] K. S. Tey, S. Mekhilef, M. Seyedmahmoudian, B. Horan, A. T. Oo, and A. Stojcevski, "Improved Differential Evolution-Based MPPT Algorithm using SEPIC for PV Systems under Partial Shading Conditions and Load Variation," IEEE Transactions on Industrial Informatics, vol.14, pp. 4322–4333, January 2018.

[22] N. Rana and S. Banerjee, "Development of an Improved Input-Parallel Output-Series Buck-Boost Converter and Its Closed-Loop Control," IEEE Transactions on Industrial Electronics, vol. 67, pp. 6428–6438, September 2020.

[23] R. Samanbakhsh, P. Koohi, F. M. Ibanez, F. Martin and V. Terzija, "A Z-source inverter with switched network in the grid-connected applications," International Journal of Electrical Power & Energy Systems, vol. 147, pp. 108819, 2023.

[24] A. Sahbani, K. Cherif and K. B. Saad, "Multiphase interleaved bidirectional DC-DC converter for electric vehicles and smart grid applications," International Journal of Smart Grid-ijSmartGrid, vol. 4, no. 2, pp. 80-7, 2020.

[25] M. H. Ibrahim, S. P. Ang, M. N. Dani, M. I. Rahman, R. Petra, and S. M. Sulthan, "Optimizing Step-Size of Perturb & Observe and Incremental Conductance MPPT Techniques Using PSO for Grid-Tied PV System," IEEE Access, vol. 11, pp. 13079–13090, February 2023.

[26] I. Owusu-Nyarko, "Classification and Comparison of Maximum Power Point Tracking Techniques in DC Micro-Grid Standalone Photovoltaic Systems," In 2024 12th International Conference on Smart Grid (icSmartGrid), pp. 747-752, IEEE, 2024.

[27] A. Harrison, N. H. Alombah and J. de Dieu Nguimfack Ndongmo, "A new hybrid MPPT based on incremental conductance-integral backstepping controller applied to a PV system under fast-changing operating conditions," International Journal of Photoenergy, vol. 2023, no. 1, pp. 9931481, 2023.

[28] K. K. Rout, D. P. Mishra, S. Mishra, S. Patra, and S. R. Salkuti, "Perturb and observe maximum power point tracking approach for microgrid linked photovoltaic system," Indonesian Journal of Electrical Engineering and Computer Science, vol. 29, no.2, pp. 635–643, February 2023.

[29] K. Ullah, M. Ishaq, F. Tchier, H. Ahmad and Z. Ahmad, "PPT) control system for photovoltaic power generation system," Results in Engineering, vol. 20, pp. 101466, 2023.

[30] L. Hichem, O. Amar and M. Leila, "Optimized ANN-fuzzy MPPT controller for a stand-alone PV system under fast-changing atmospheric conditions," Bulletin of Electrical Engineering and Informatics, vol. 12, no. 4, pp. 1960-1981, 2023.

[31] S. Rafi Kiran and F. Alsaif, "A novel advanced hybrid fuzzy MPPT controllers for renewable energy systems," Scientific Reports, vol. 14, no. 1, pp. 21104, 2024.

[32] S. R. Kiran, C. H. Basha, V. P. Singh, C. Dhanamjayulu, B. R. Prusty, and B. Khan, "Reduced simulative performance analysis of variable step size ANN based MPPT techniques for partially shaded solar PV systems," IEEE Access, vol. 10 pp. 48875–48889, May 2022.

[33] F. Nejabatkhah, S. Danyali, S. H. Hosseini, M. Sabahi, and S. M. Niapour, "Modeling and control of a new three-input DC–DC boost converter for hybrid PV/FC/battery power system," IEEE Transactions on power electronics, vol. 27, no. 5, pp. 2309–2324, November 2011.

[34] F. Galea, M. Apap, C. S. Staines, and J. Cilia, "Design of a high efficiency wide input range isolated Cuk Dc-Dc converter for grid connected regenerative active loads," 2011.

[35] P. Javeed, L. K. Yadav, P. Venkatesh Kumar, R. Kumar, and S. Swaroop, "SEPIC Converter for Low Power LED Applications," In Journal of Physics: Conference Series, vol. 1818, no. 1, pp. 012220, March 2021.

[36] J. C. Rosas-Caro, F. Z. Peng, H. Cha, and C. Rogers, "Z-source-converter-based energy-recycling zero-voltage electronic loads," IEEE Transactions on Industrial Electronics, vol. 56, no.12, pp. 4894–4902, July 2009.

[37] A. R. Youssef, H. Ramadan, H. H. Mousa, and E. E. Mohamed, "An efficient variable-step P&O maximum power point tracking technique for grid-connected wind energy conversion system," SN Applied Sciences, vol. 1, pp. 1–15, December 2019.

[38] M. A. Elsaharty, N. E. Zakzouk, A. K. Abdelsalam, A. A. Helal, and B. W. Williams, "Improved performance low-cost incremental conductance PV MPPT technique," IET Renewable Power Generation, vol. 10, no. 4, pp. 561–574, April 2016.

[39] A. K. Raji and D. N. Luta, "Fuzzy rule-based and particle swarm optimisation MPPT techniques for a fuel cell stack," Energies, vol. 12, no. 5, pp. 936, March 2019.